




Advanced Postirradiation Characterization of Nuclear Fuels Using Pulsed Neutrons

SVEN C. VOGEL ^{1,9} MARK A.M. BOURKE,¹ AARON E. CRAFT,²
JASON M. HARP,^{2,3} CHARLES T. KELSEY,⁴ JAY LIN,⁵
ALEX M. LONG,¹ ADRIAN S. LOSKO,^{1,6} PETER HOSEMANN,⁵
KENNETH J. MCCLELLAN,¹ MARKUS ROTH,⁷ and ANTON S. TREMSIN⁸

1.—Material Science and Technology Division, Los Alamos National Laboratory, Los Alamos, NM 87545, USA. 2.—Materials and Fuels Complex, Idaho National Laboratory, Idaho Falls ID 83415, USA. 3.—Reactor and Nuclear Systems Division, Oak Ridge National Laboratory, Oak Ridge, TN 37831, USA. 4.—Physics Division, Los Alamos National Laboratory, Los Alamos NM 87545, USA. 5.—Nuclear Engineering Department, University of California Berkeley, Berkeley, CA 94720, USA. 6.—Forschungs-Neutronenquelle Heinz Maier-Leibnitz (FRM II), 85748 Garching b. München, Germany. 7.—Nuclear Physics Institute, Technische Universität Darmstadt, 64289 Darmstadt, Germany. 8.—Space Science Laboratory, University of California Berkeley, Berkeley, CA 94720, USA. 9.—e-mail: sven@lanl.gov

Methods for postirradiation characterization of bulk (cm^3) irradiated materials or even spent nuclear fuels are sparse due to their extremely radioactive nature. While several methods exist to characterize smaller volumes ($< 1 \text{ mm}^3$) of such samples, selecting these volumes from larger samples is challenging. X-ray-based methods are prohibitive due to the strong γ -radiation from the sample flooding the detectors. Neutron-based methods available in the proximity of irradiation reactors allow for thermal neutron radiography or computed tomography using a small reactor source, but one cannot assess isotope distributions or microstructural features such as phases, texture, or strain from diffraction measurements due to flux limitations. We present herein a pathway to provide pulsed neutron characterization of bulk irradiated samples using time-of-flight neutron diffraction for microstructural characterization and energy-resolved neutron imaging for assessment of isotopic densities and distributions. Ultimately, laser-driven pulsed neutron sources may allow deployment of these techniques pool-side at irradiation reactors.

INTRODUCTION

A key enabler for a science-based approach to accelerated development and certification of new nuclear fuels is an early and efficient understanding of material behavior at multiple length scales. For new fuel formulations, there is a dearth of irradiation testing experience. When representative irradiation tests take years and the postirradiation characterization is costly, it is important to extract the maximum insight possible from each test. Postirradiation examination (PIE) of fuels is mature and sophisticated, but measurements in hot cells are expensive and typically examine small volumes of irradiated fuels, relying on a limited amount of knowledge of the bulk characteristics of the specimen to select the volume examined destructively.

This leaves the possibility that key failure-inducing phenomena will not be observed because of limited *bulk* PIE. For these reasons, there is value in techniques that can quickly and nondestructively characterize properties over volumes consistent with standard fuel geometries. Applying such methods pre- and postirradiation unambiguously determines the changes induced by irradiation. Preirradiation examination implies that these techniques are non-destructive. Such techniques can inform models on the initial condition of samples and complement, guide, and leverage destructive postirradiation examination; For example, three-dimensional characterization of complete fuel pellets within cladding after irradiation could identify regions that are representative of the average response with parameters not accessible by presently applied techniques

such as visual inspection, thermal neutron radiography, or acoustic methods. At the same time, providing information over the entire sample volume allows one to also identify deviations from the average and typical behavior that can be further investigated by more local characterization techniques after the volume is prepared out of the entire pellet using destructive techniques.

Typical in-pile irradiation tests of new fuel types last months or years. The resulting levels of radioactivity even for rodlets containing just a handful of pellets or metallic fuels of less than 1 cm^3 in volume require hot cells and remote manipulators to perform destructive PIE. The complexity and cost of such operations limit the PIE possible, thus there is a premium on knowing where to measure by identifying regions of interest by as many nondestructive characterizations as possible. Only a few examples of neutron characterization of irradiated or even spent fuels are reported in the literature: At the Intense Pulse Neutron Source (IPNS) at Argonne National Laboratory, irradiated U_3Si_2 and U_3Si were characterized in the 1990s.¹⁻³ At the Paul-Scherrer-Institute, capabilities for neutron imaging characterization of highly radioactive materials were developed in the early 2000s^{4,5} and applied to postirradiation characterization of target rods of the SING spallation neutron source.⁶ More recently, at the Chalk River reactor high-burnup, nuclear fuel from the same reactor was characterized by neutron diffraction.⁷

The programmatic emphases for developing advanced nondestructive evaluation (ANDE) techniques applicable to irradiated materials are twofold. First, it will be possible to evaluate fuel materials to guide the destructive postirradiation examination towards regions of interest that are not obvious with conventional techniques. This will help develop the statistical insight necessary to complement modeling and simulation data. Adding ANDE insight to the standard optical, thermal neutron, and gamma ray insights will help identify regions where destructive examination can be focused. This will increase the return from postirradiation examination, since regions of atypical irradiation performance are more likely to be discovered. A second reason for ANDE lies in the desire to generate data as soon as possible after removal of the test samples from the reactor. This is a key requirement in accelerating the development and time to licensing of new fuel forms. This philosophy is consistent with improving diagnostics to offer faster turnaround and getting “more out of less.” Programmatically, the capabilities under development set the stage for routine preirradiation fuel evaluation and potentially for postirradiation evaluations of accident-tolerant fuels (ATFs)⁸⁻¹¹ and fast neutron spectrum reactor transmutation fuels.¹²⁻¹⁶

The research presented herein focused on developing techniques for nondestructive examination of the bulk volume of rodlets containing multiple

pellets or metallic fuels of similar dimensions. Furthermore, a path towards deploying these capabilities currently requiring a large-scale user facility such as the Los Alamos Neutron Science Center (LANSCE) at Los Alamos National Laboratory (LANL) to allow for pool-side characterization at the irradiation reactor using laser-driven neutron sources is also outlined. The first step in this project is to benchmark the initial condition of candidate materials before irradiation. This has been done at LANSCE on all available fuel forms such as conventional UO_2 fuel pellets,¹⁷ accident-tolerant $\text{UN}/\text{U}_3\text{Si}_5$ and U_3Si_2 fuels,^{18,19} metallic U-Zr ,²⁰ and U-Mo ^{21,22} fuels as well as transmutation fuels such as U-Pu-Zr systems.²³ The second step will be to make comparable measurements on irradiated rodlets prior to their destructive examination in Idaho National Laboratory (INL) hot cells. Neutron, proton,²⁴ and (synchrotron) x-ray²⁵ radiography/tomography and diffraction techniques all provide opportunities for this endeavor. By virtue of their stand-off capability and ability to probe materials despite an intense gamma field, neutrons and protons both offer potential for study of highly radioactive materials. An initial design of a handling cask allowing such neutron characterization is presented.

The techniques employed at LANSCE use the pulsed neutron source at the Lujan Center, relying on co-location with the 800-MeV proton accelerator.²⁶ However, advances in small-scale accelerators for neutron generation (by D-D fusion) or laser-driven pulsed neutron sources^{27,28} provide interesting opportunities.²⁹ Although such small-scale sources are not currently capable of neutron production for measurements of the type described here, technological advances are ongoing. It is possible that, in the next decade, a “small-scale” accelerator source with sufficient neutron production performance might become available to provide poolside implementation of the techniques described here.³⁰

EXPERIMENTAL PROCEDURES

This section provides brief descriptions of the capabilities involved and the instruments utilized, as well as a description of the initial design of a cask that allows handling and characterization of irradiated nuclear fuels in the future.

Facilities at Idaho National Laboratory (INL)

Facilities located at INL include fuel fabrication, preirradiation characterization, irradiation at the Advanced Test Reactor (ATR), and postirradiation examination at various facilities located at INL's Materials & Fuels Complex (MFC).³¹ Fuels and other nuclear materials fabricated at the Materials & Fuels Complex or elsewhere are sent to the Advanced Test Reactor, where they are irradiated under representative or prototypic conditions. The

irradiated fuels are then returned to the Hot Fuels Examination Facility (HFEF) at the Materials & Fuels Complex, where they undergo a variety of nondestructive examinations prior to destructive examinations. Irradiated fuels studied at INL are often fabricated and irradiated on site. In addition, INL is also able to receive nuclear fuels irradiated at other reactors for examination.^{32–37} Once the irradiated fuels arrive at the Hot Fuels Examination Facility, nondestructive examinations that may be performed include visual examination, neutron radiography and tomography, dimensional inspection and profilometry, precision gamma scanning (PGS), and eddy-current examination.³⁸ It is pertinent to mention that the neutron radiography and CT capabilities currently available at the Hot Fuels Examination Facility^{39–41} do not assess isotope distributions or microstructural features such as crystallographic phases, texture, or strain, which might be accessible using pulsed neutron characterization. The neutron radiography and tomography capabilities at NRAD have expanded to include digital camera/scintillator-based neutron imaging systems currently capable of imaging some irradiated nuclear fuels with up to 2 Sv/h at the scintillator screen, and ongoing developments are seeking to expand these capabilities to withstand even higher dose rates to enable digital neutron tomography of highly radioactive fuels as a routine PIE technique.^{42,43} These nondestructive examinations inform researchers about locations suitable for subsequent detailed destructive examinations. Samples may be prepared for metallography/ceramography, physical properties testing (e.g., thermal properties, density), chemical analysis, isotopic analysis, alpha/beta/gamma spectrometry, mass spectrometry techniques, mechanical property testing, and

other analyses. These examination capabilities are available at other facilities co-located at the Materials & Fuels Complex.

Facilities at Los Alamos National Laboratory (LANL)

At present, the pulsed neutron methods described here require large-scale user facilities such as LANSCE. Besides providing the required neutron instruments, these facilities also have to have the authorization basis, infrastructure, and experience to handle such materials. While international shipment of such materials is not impossible, for example, the spallation neutron source at J-PARC, Tokai, Japan, is not authorized to handle even depleted uranium. Handling of these materials in the USA is regulated by a materials at risk (MAR) assessment of the samples.^{44,45} This assessment takes into consideration several hazard management aspects of the materials, including radioactivity, and results in a MAR expressed in “plutonium equivalent grams” (PEG). Facilities have designated MAR limits for their total inventory. At LANSCE, the Manuel Lujan Scattering Center, where HIPPO and ERNI described below are located, has a MAR limit of 380 PEG, while the Weapons Neutron Research (WNR, unmoderated spallation neutrons) and proton radiography (pRAD) facilities at LANSCE have limits of 40 PEG and 12 PEG, respectively. For comparison, the SNS requires case-by-case approval by the Department of Energy for experiments involving MAR samples. In this combination of pulsed neutron characterization capabilities with an authorization basis that allows handling of all fuel forms, LANSCE at LANL is unique worldwide. The capability to characterize MAR samples is, for example, documented by the characterization of a

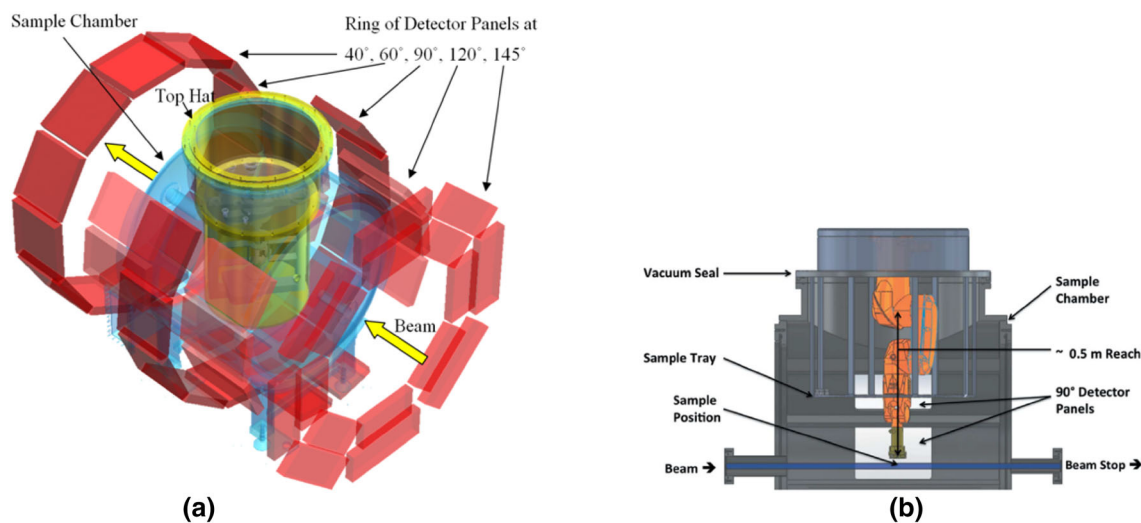


Fig. 1. Schematics of the HIPPO instrument (a) and the robotic sample changer (b).

U-20Pu-10Zr-3Am-2Np sample, a sample classified as a material at risk sample of 18.0 PEG.²³

Neutron Diffraction

For time-of-flight neutron diffraction characterization of nuclear fuels, the High Pressure/Preferred Orientation (HIPPO) beamline at LANSCE is utilized.^{46,47} Figure 1a provides a schematic of the instrument. The comparably short distance of 8.83 m between moderator and sample combined with the comparably large detector coverage of 22.4% of the sphere around the sample⁴⁸ provides for efficient neutron characterization. A robotic sample changer⁴⁹ is used to handle samples inside the instrument (Fig. 1b). In combination with a 2-mm Cd slit to define a slice of the sample, the robotic arm allows to scan rodlets with several pellets in 2-mm slices, thus providing limited spatial resolution for the diffraction. Data analysis is conducted using the Rietveld method, fitting every experimental data point to a complex (several tens of parameters) model taking into account instrument parameters (e.g., time-of-flight to d -spacing conversion, background, instrument peak broadening), crystallographic parameters (e.g., lattice parameters, atomic positions, atomic displacement parameters), and microstructural parameters (texture/preferred orientation, phase fractions, defect concentrations). Figure 2a shows an example of a Rietveld analysis of a 2-mm slice of a UN/U₃Si₅ sample inside a stainless-steel rodlet. Figure 2b shows the refined unit cell volume (many other refined parameters are omitted here) of the hexagonal crystal structure of U₃Si₅ as a function of sample position along the rodlet. The data points corresponding to the lowest pellet are significantly below those of the other pellets, indicating an anomaly for this particular pellet. Measurement of the crystal orientation distribution (texture, preferred orientation) shows that, while the UN crystals show the expected random orientation distribution (absence of preferred orientation), the U₃Si₅ shows a very strong texture consistent with essentially two single crystals within the probed volume. This can be explained based on the fact that, during sintering, this particular pellet was unintentionally exposed to a temperature slightly higher than the melting point of U₃Si₅. Upon cooling, the U₃Si₅ solidified in an interconnected network surrounding the UN grains, but forming the two single crystals seen now. It is worth pointing out that this pellet, fabricated during the development of synthesis routes for this particular fuel form, passed visual inspection and did not show any differences in density prior to insertion into the capsule. Anisotropic thermal expansion along the crystallographic a - and c -axes of the hexagonal crystal lattice may lead to thermal stresses that could cause cracking of this pellet during heating, significantly changing the behavior during irradiation. This example

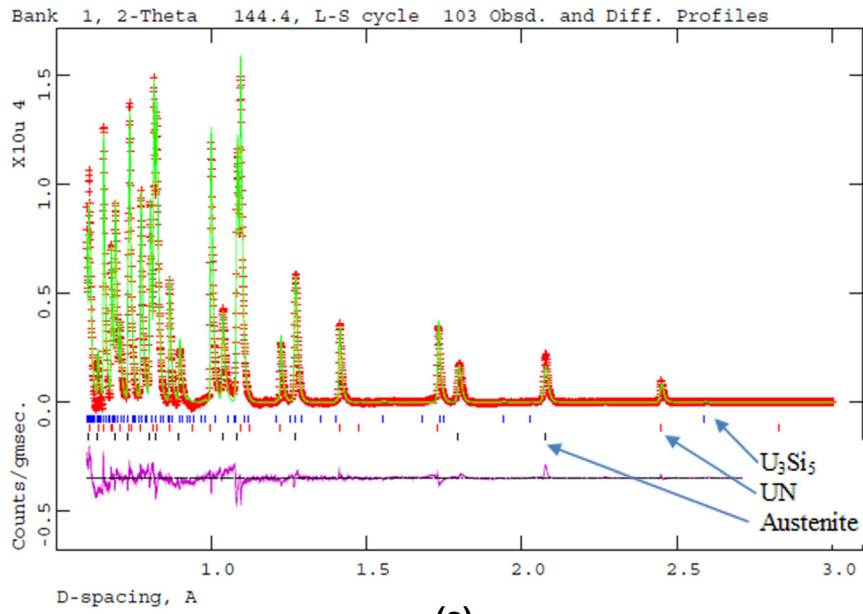
Fig. 2. (a) Example of Rietveld full pattern diffraction data analysis of HIPPO data on UN/U₃Si₅ composite fuel inside stainless-steel cladding. The red crosses are measured intensities, the green line is the Rietveld fit, and the tick marks below the pattern label calculated peak positions for the phases indicated. The difference curve for the data shown as intensity versus d -spacing is shown below. (b) Unit cell volume of the hexagonal U₃Si₅ phase resulting from lattice parameter refinements as a function of scan height, indicating that the data points corresponding to the first of the three pellets scanned are significantly lower than the average. (c) Pole figures of texture analysis measuring the grain orientation in the probed volume. While the UN grains show random grain orientation (absence of preferred orientation), these data indicate that the U₃Si₅ phase has a microstructure similar to a single crystal with essentially two main orientations for crystallographic c -axes (002 pole figure) and two sets of maxima for each of the three a -axes (200 pole figure) visible for each orientation.

underlines the value that bulk neutron characterization can provide for preirradiation characterization, but also for the development of fabrication routes. Besides pre- and postirradiation characterization, neutron diffraction also has significant advantages for the characterization of the crystal and microstructure evolution of nuclear fuels at temperature, atmosphere, processing route, etc., e.g. for separate effect testing.

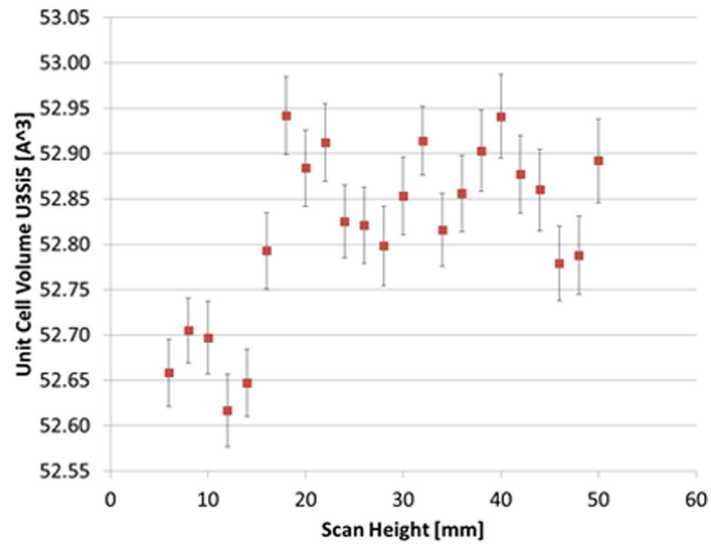
Energy-Resolved Neutron Imaging and Computed Tomography

Located next to the HIPPO beamline is the energy-resolved neutron imaging (ERNI) beamline on flight path 5⁵⁰ at the Lujan Center. Similar to HIPPO, the ERNI beamline takes advantage of the same pulsed neutrons coming from the high-intensity moderator on the 1L target.⁵¹ For a schematic layout of the ERNI beamline on flight path 5, see Fig. 3a. Using this pulsed neutron source, along with a pixilated neutron time-of-flight detector, neutron radiographs can be further separated out based on the time of arrival, or energy, of each incoming neutron (Fig. 3b). The detector used for ERNI measurements consists of neutron-sensitive microchannel plates (MCPs) coupled to four Timepix readout chips [see schematic in (Fig. 3c), combining to form a total active area of 28 mm × 28 mm.^{52,53} This type of detector setup is capable of producing highly pixilated (512 × 512 at 55- μ m pitch) neutron radiographs at frame rates above 60 kHz, or roughly 3000 frames per neutron pulse at the Lujan Center. Combining this type of detector with the pulsed neutron source at the Lujan Center opens up avenues for several novel applications for material characterizations, ranging from specific isotope mapping¹⁷ to bulk temperature mapping.⁵⁴

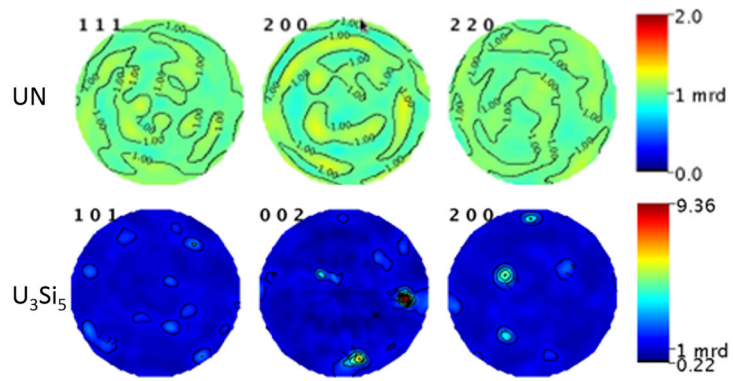
A typical energy-resolved neutron imaging experiment involves transmission measurements, where neutrons passing through a given sample interact with the material based on neutron cross-sections of the isotopic constituents within the material. These



(a)



(b)



(c)

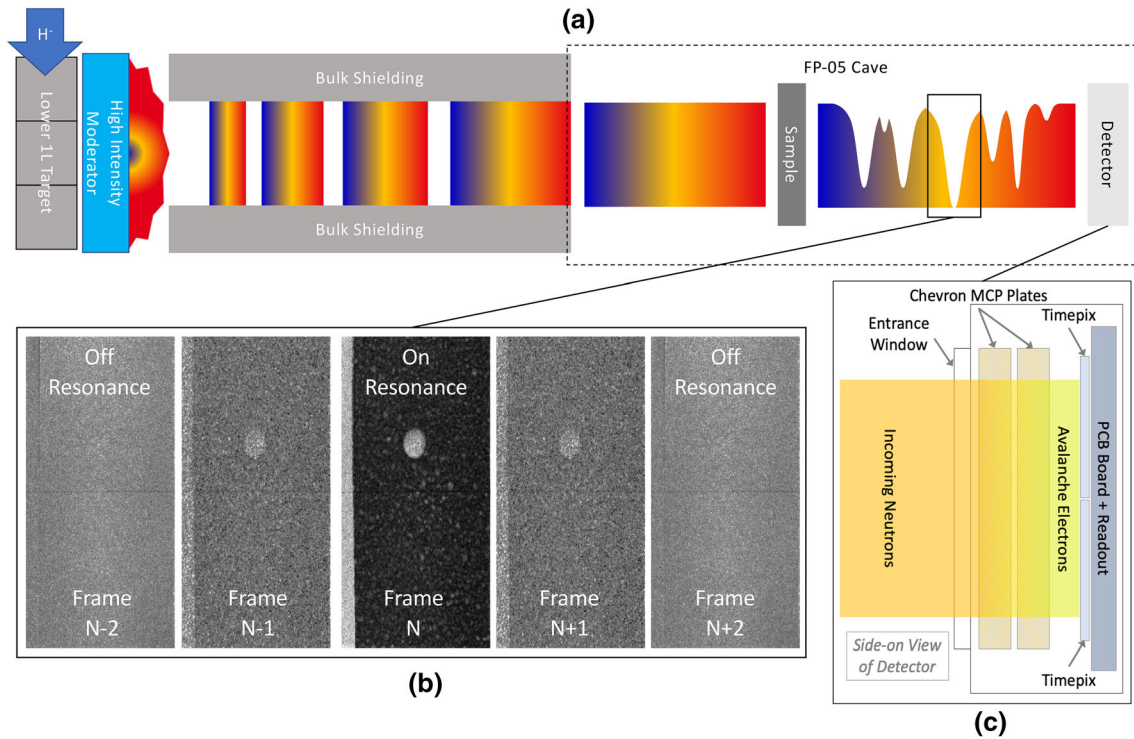


Fig. 3. (a) Schematic of flight path 5. (b) Examples of radiographs collected at energies around a neutron absorption resonance. (c) Schematic of the pixilated time-of-flight imaging detector.

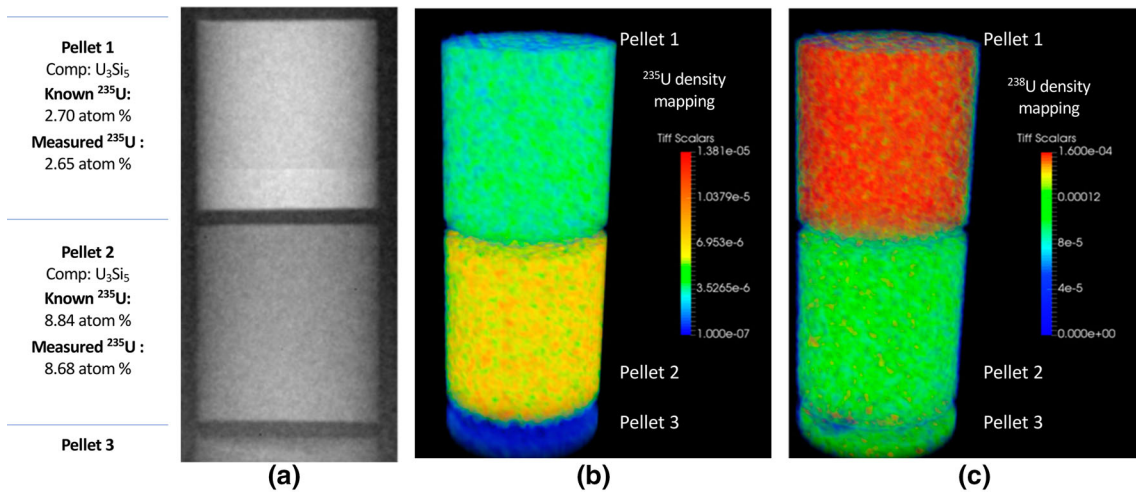


Fig. 4. Thermal neutron radiography (a) and reconstruction of ^{235}U (b) and ^{238}U (c) isotope densities.

interactions absorb a certain number of neutrons at specific energies, so-called neutron absorption resonances, as they pass through the sample, thus resulting in observable dips in the transmission spectrum recorded by a time-of-flight (TOF) detector at these energies. The depth and position of these transmission dips act as a fingerprint for the isotopic composition of the sample. Using modern reaction-theory codes, such as SAMMY⁵⁵ or REFIT,⁵⁶ transmission spectra can be fit as a function of energy to extract quantities such as

isotopic areal densities. This transmission fitting procedure can be done on a pixel-by-pixel basis, thus producing a two-dimensional (2D) map of specific isotopic density distributions for each isotope within the sample. Furthermore, by recording and extracting 2D isotopic densities over a range of sample rotations, a three-dimensional (3D) isotopic distribution map can be obtained through computed-tomography techniques. An example of this is shown in Fig. 4, where UN/U-Si composite fuels were imaged using ERNI techniques over ~ 60

sample rotations. Transmission spectra with absorption resonances from ^{235}U and ^{238}U within the transmission spectra were fit using SAMMY to extract areal densities of ^{235}U and ^{238}U for each pixel in each sample rotation image. These isotopic density maps of ^{235}U and ^{238}U are processed by CT reconstruction software⁵⁷ to ultimately create 3D density maps of ^{235}U and ^{238}U within the imaged pellets. It has been demonstrated that this technique can not only be qualitative, but also a quantitative probe in actually measuring isotopic contents at fractions of atomic percent levels.²³

Recently, it was demonstrated that neutron radiography of irradiated fuel assemblies can be performed with an equivalent detector system despite the very intense radiation fields produced by the fuel that make their postirradiation examination very difficult.^{58,59} The neutron imaging detector, equivalent to the one used at the FP5 beamline, comprising microchannel plates (MCPs) and a Timepix readout, was tested in intense gamma and neutron radiation environments on a beamline at the Neutron Radiography Reactor (NRAD) at Idaho National Laboratory. Initially, neutron radiography experiments of nonirradiated materials were performed with the detector installed 17.5 m from the reactor core in a line-of-sight view to the core of the reactor. Therefore, the detector was exposed to a fast and epithermal neutron spectrum as well as high-intensity gamma radiation.⁶⁰ The gamma-ray dose rate in the beam line was 812 mSv/h. Complementary measurements were made using ^{137}Cs and ^{60}Co isotopic sources at gamma dose rates in excess of 6 Sv/h. The detector functioned normally over several hours in this environment. These measurements were followed by the imaging of an irradiated fuel assembly with the detector installed at 4.8 m from the reactor core, again with a direct view onto the reactor core. A 75-cm-long irradiated fuel assembly was positioned ~ 4 cm from the detector during neutron radiography. The radiation generated by the fuel assembly at the detector position was 5.48 Sv/h. A set of neutron transmission images was acquired by the detector, which could operate in these high-radiation environments despite several single-event upsets observed in the field-programmable gate array (FPGA) processing electronics. These experiments demonstrated that high-resolution imaging of irradiated fuel assemblies is possible with digital detectors, which can extend the capabilities of nondestructive studies to many advanced imaging techniques such as tomography, resonance absorption, Bragg-edge imaging, dark-field imaging, and others. These conditions are comparable to planned radiography of irradiated nuclear fuel assemblies, but with a pulsed source, the time during which the detector is active can be reduced to the neutron time of flight of interest, thus greatly improving the signal-to-noise ratio.

Handling Cask

In a collaboration between LANL, INL, and University of California, Berkeley, a container for nuclear-irradiated fuel rodlet transportation and nondestructive tomography imaging as well as time-of-flight neutron diffraction is currently being developed, the Radioactive Material Handling Mechanism (RaMHaM). The proposed container design has four main components: shielding structures, pneumatic shutters, a center plug, and a rodlet adaptor (Fig. 5). In the current design, the main shielding structure contains a 0.25-inch stainless-steel frame with an average of 4 inches of cast-lead fill-ins in lateral thickness. Further shielding analysis is on-going for further validation of the radiation attenuation assumption. The design also integrates a shutter mechanism. When the container aligns with the neutron beam in the beamline, the pneumatic shutters can be remotely controlled to expose and close the imaging window as well as beam paths for 90° diffraction. The container has only one open end, fit with a center plug stopper to reduce the potential for radiation leakage. The center plug also hosts the irradiated fuel rodlet adaptor and the fuel rodlet. When installing the rodlet into the container in a hot cell, operators can attach the rodlet to the custom-designed adaptor and secure it onto the shaft in the center plug. Stepper motors can be attached to the shaft for positioning the rodlet vertically as well as for providing rotation for the neutron characterization.

Commercial type B casks such as the BEA Research Reactor (BRR) cask are certified by the Nuclear Regulatory Commission (NRC) to carry radioactive payload on open roads. The design of RaMHaM will allow it to fit into such casks, enabling transport between national laboratories.

Laser-Driven Neutron Sources

Transport of irradiated samples between irradiation and characterization facilities is expensive and cumbersome. A facility such as LANSCE requires investment in excess of US \$1B with concurrent operational cost for linear proton accelerator and target systems, therefore lying out of reach for deployment at, e.g., INL in proximity to the Advanced Test Reactor as a characterization tool. However, recently, laser-driven neutron sources may have opened an opportunity to provide LANSCE-like neutron flux on samples at greatly reduced investment and operational costs. As illustrated in Fig. 6, in a laser-driven neutron source, particles are accelerated by an intense ($> 10^{21}$ W/cm²) laser pulse impinging on a thin-film target, sweeping a large fraction of the electrons outside the surface on the opposite side of the laser. The resulting electric field on the order of TV/m accelerates the remaining cations of the target material

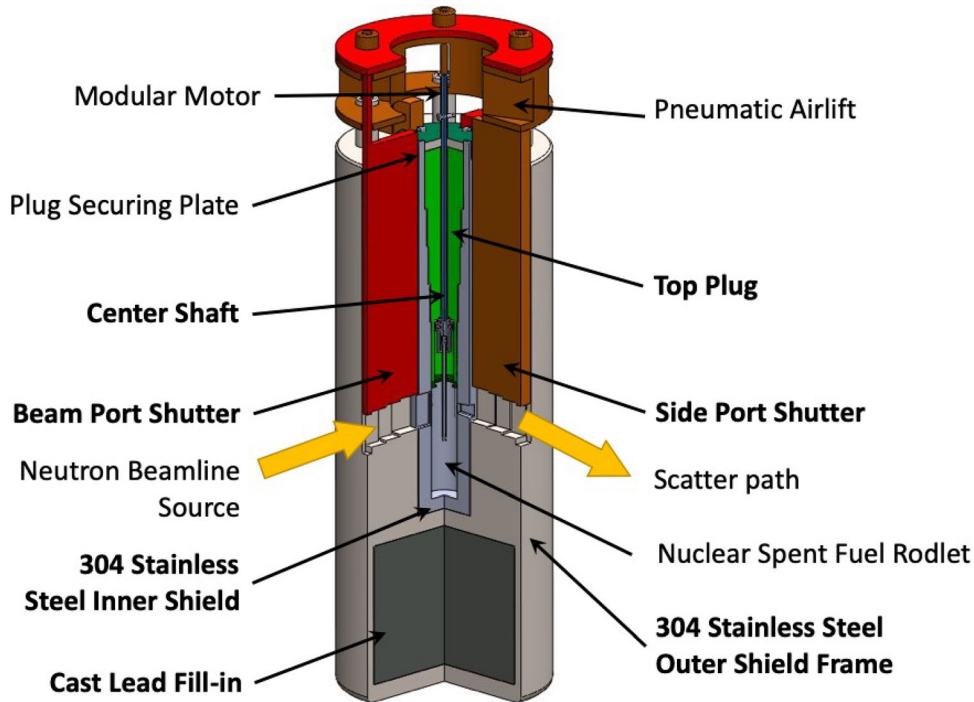


Fig. 5. Isoview of the Radioactive Material Handling Mechanism (RaMHaM).

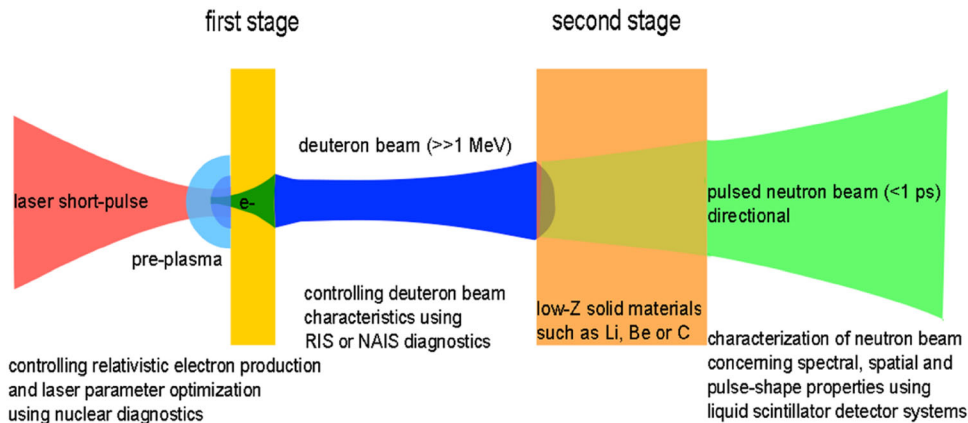


Fig. 6. Schematic of the process of laser-driven neutron production. See text for details.

(so-called target sheath-normal acceleration^{27,28}). Coupling of an appropriately shaped laser pulse with the electrons remaining in the target accelerates these electrons to become relativistically heavy on the order of the cations, suppressing the interaction of the laser photons with the electronic shells and making the remaining target material relativistically transparent. This allows coupling of the laser pulse with the cations, which in turn are, besides acceleration by the electric field caused by the electrons outside the thin-film target, also accelerated by the laser pulse, via the so-called break-out afterburner (BOA) effect.⁶¹ For a deuterated polymer target of appropriate thickness, this results in a deuteron pulse of ~ 20 MeV traveling in the direction of the incident laser pulse. A

suitable ~ 1 -cm target, typically Be, in the path of this deuteron pulse several millimeters from the thin-film target for the laser allows conversion of the deuterons into neutrons. This occurs predominantly by the deuteron break-up reaction, which is not a nuclear reaction via an excited state of the target nucleus, and therefore the momentum of the incoming deuterons is preserved, providing a neutron pulse predominantly traveling in the direction of the original laser pulse.^{27,28} This can be readily captured in a moderator, avoiding the losses of ~ 2 orders of magnitude between target and moderator in the isotropic spallation process using, for example, the 20-cm-long tungsten spallation target at the Manuel Lujan Neutron Scattering Center,⁵¹ leading to a two orders of magnitude larger fraction of the

produced neutrons becoming available at the sample position in case of a laser-driven neutron source. By changing a deuterated polymer foil and Be target for neutron production with a conventional protonated polymer foil and a high- Z -material target, such as a tungsten target, MeV x-rays of subnanosecond duration can be produced. Initial tests with the TRIDENT laser at LANL indicate that these pulses originate from a source size smaller than $\sim 100 \mu\text{m}$.²⁸ This is at least one order of magnitude smaller than x-rays produced by Bremsstrahlung in conventional microtron x-ray sources, allowing one to magnify the object under examination in x-ray radiography or CT. Similarly, using the unmoderated fast neutrons for radiography applications provides a small source size not possible with conventional neutron sources. The compactness of a laser-driven setup would allow interchangeable targets, providing multimodal characterization of objects such as irradiated fuels without the need to move the sample.

While conventional proton or deuteron acceleration in electromagnetic fields for neutron production is limited by an upper physical limit for the charge per volume,⁶² acceleration utilizing sub-picosecond photon pulses with charged particles, only experiencing repulsion on similar sub-picosecond time scales before being converted to neutrons, allows one to surpass this limit. Furthermore, the initial investment and operational costs of such a laser-driven neutron source are expected to be also about two orders of magnitude below those of a conventional spallation neutron source.⁶³ This will likely allow deployment of LANSCE-like neutron sources as sophisticated characterization tools at irradiation facilities, significantly increasing the pre- and postirradiation characterization capabilities and therefore accelerating development and licensing of advanced nuclear fuels.

CONCLUSION

The methods presented here provide a set of tools that will ultimately allow characterization of the entire irradiated volume within a standard irradiation capsule for parameters including:

- Voids, cracks, pellet-to-cladding distances, etc. using epithermal neutrons not suffering the strong absorption of thermal and cold neutrons by fissionable material. Ultimately, intense subnanosecond-long MeV x-ray or MeV fast neutron pulses originating from $< 50 \mu\text{m}$ source size from a laser-driven source in combination with gated imaging detectors will allow to overcome the intense gamma radiation emitted from the samples for additional radiography and CT modalities. Development of combined CT reconstruction codes, utilizing these different interaction physics to characterize the same voxel, is ongoing.

- Isotope densities from neutron absorption resonance analysis that will provide absolute isotope densities of fission products, including fission gases,⁶⁴ on a $\sim 100\text{-}\mu\text{m}$ resolution. Routine 3D mapping of densities of fission products will provide benchmarking of burnup simulation codes predicting these quantities that are hitherto only very rarely if at all available.
- For samples allowing penetration by thermal neutrons, such as fuels with less than $\sim 5\%$ enrichment level (low enriched), microstructural parameters such as qualitative and quantitative phase analysis, texture, and defect densities can be assessed in millimeter slices along the axis of the irradiation capsule using neutron diffraction.
- Infrastructure to handle irradiated fuels in a cask designed for neutron characterization at LANSCE is under development.

All of the aforementioned information can be compared with the equivalent preirradiation datasets, thus providing unprecedented pre- and postirradiation comparison of the entire irradiated volume. Nondestructive preirradiation characterization of the entire irradiation capsule adds both baseline data as well as quality checks. Furthermore, the information can ensure that the most rewarding smaller volumes are prepared destructively from the irradiated volume for more local, smaller length scale investigation using other techniques.

ACKNOWLEDGEMENTS

This work was supported by the DOE/NE Fuel Cycle R&D research program. This work has benefited from the use of the Los Alamos Neutron Science Center (LANSCE) at Los Alamos National Laboratory. Los Alamos National Laboratory is operated by Triad National Security, LLC, for the National Nuclear Security Administration of the U.S. Department of Energy under Contract No. 89233218NCA000001.

REFERENCES

1. R.C. Birtcher, J.W. Richardson, and M.H. Mueller, *J. Nucl. Mater.* 230, 158 (1996).
2. J.W. Richardson Jr, R.C. Birtcher, and S.K. Chan, *Phys. B: Cond. Matter.* 241, 390 (1997).
3. R.C. Birtcher, J.W. Richardson Jr, and M.H. Mueller, *J. Nucl. Mater.* 244, 251 (1997).
4. E.H. Lehmann, P. Vontobel, and L. Wiesel, *Nondestr. Test. Eval.* 16, 203 (2001).
5. E.H. Lehmann, P. Vontobel, and A. Hermann, *NIMA* 515, 745 (2003).
6. P. Vontobel, M. Tamaki, N. Mori, T. Ashida, L. Zanini, E.H. Lehmann, and M. Jaggi, *J. Nucl. Mater.* 356, 162 (2006).
7. D. Sears, N. Wang, R. Rogge, I. Swainson, and R. Donabarger, CNBC report CNBC-2011-MS-5 (2011).
8. J. Carmack and F. Goldner, *J. Nucl. Mater.* 448, 373 (2014).
9. K.E. Barrett, K.D. Ellis, C.R. Glass, G.A. Roth, M.P. Teague, and J. Johns, *Nucl. Eng. Des.* 294, 38 (2015).
10. F. Cappia, J.M. Harp, and K. McCoy, *J. Nucl. Mater.* 517, 97 (2019).
11. F. Cappia and J.M. Harp, *J. Nucl. Mater.* 518, 62 (2019).
12. J.M. Harp, S.L. Hayes, P.G. Medvedev, D.L. Porter, and L. Capriotti, Idaho Natl. Lab. Rep. INL/EXT-17-41677 (2017).

13. P. Medvedev, S. Hayes, S. Bays, S. Novascone, and L. Capriotti, *Nucl. Eng. Des.* 328, 154 (2018).
14. J.M. Harp, H.J.M. Chichester, and L. Capriotti, Idaho Natl. Lab. Rep. INL/LTD-16-40088 (2016).
15. J.M. Harp, L. Capriotti, H.J.M. Chichester, P.G. Medvedev, D.L. Porter, and S.L. Hayes, *J. Nucl. Mater.* 509, 454 (2018).
16. J.M. Harp, H.J.M. Chichester, and L. Capriotti, *J. Nucl. Mater.* 509, 377 (2018).
17. A.S. Tremsin, S.C. Vogel, M. Mocko, M.A. Bourke, V. Yuan, R.O. Nelson, D.W. Brown, and W.B. Feller, *J. Nucl. Mater.* 440, 633 (2013).
18. M.A. Bourke, S.C. Vogel, S.L. Voit, K.J. McClellan, A.S. Losko, and A.S. Tremsin, Los Alamos National Laboratory report LA-UR-16-22179 (2016).
19. S.C. Vogel, N.P. Borges, A.S. Losko, S.M. Mosby, S.L. Voit, J.T. White, D.D. Byler, J.T. Dunwoody, A.T. Nelson, and K.J. McClellan, Los Alamos National Laboratory report LA-UR-17-28837 (2017).
20. S. Irukuvarghula, B. Blamer, S. Ahn, S.C. Vogel, A.S. Losko, and S.M. McDevitt, *J. Nucl. Mater.* 497, 10 (2017).
21. S. Takajo, K.J. Hollis, D.R. Cummins, E.L. Tegtmeier, D.E. Dombrowski, and S.C. Vogel, *Quantum Beam Sci.* 2, 12 (2018).
22. K.J. Hollis, D.R. Cummins, S.C. Vogel, and D.E. Dombrowski, *J. Therm. Spray Technol.* 28, 314 (2019).
23. S.C. Vogel, D.D. Byler, E. Kardoulaki, A.S. Losko, K.J. McClellan, A.S. Tremsin, A.D.R. Andersson, and J.T. White, Los Alamos National Laboratory report LA-UR-18-24874 (2018).
24. C.L. Morris, M.A.M. Bourke, D.D. Byler, C.F. Chen, G. Hogan, J.F. Hunter, K. Kwiatkowski, F.G. Mariam, K.J. McClellan, F. Merrill, and D.J. Morley, *Rev. Sci. Instrum.* 84, 023902 (2013).
25. R. Pokharel, D.W. Brown, B. Clausen, D.D. Byler, T.L. Ickes, K.J. McClellan, R.M. Suter, and P. Kenesei, *Microsc. Today* 25, 42 (2017).
26. P.W. Lisowski and K.F. Schoenberg, *NIMA* 562, 910 (2006).
27. M. Roth, D. Jung, K. Falk, N. Guler, O. Deppert, M. Devlin, A. Favalli, J.C. Fernandez, C.D. Gautier, M. Geissel, and R. Haight, *Phys. Rev. Lett.* 110, 044802 (2013).
28. J.C. Fernández, D.C. Gautier, C. Huang, S. Palaniyappan, B.J. Albright, W. Bang, G. Dyer, A. Favalli, J.F. Hunter, J. Mendez, and M. Roth, *Phys. Plasmas* 24, 056702 (2017).
29. M. Roth, S.C. Vogel, M.A.M. Bourke, J.C. Fernandez, M.J. Mocko, S. Glenzer, W. Leemans, C. Siders, and C. Haefner, Los Alamos National Laboratory report LA-UR-17-23190 (2017).
30. U. Rücker, T. Cronert, J. Voigt, J.P. Dabruck, P.E. Doege, J. Ulrich, R. Nabbi, Y. Beßler, M. Butzek, M. Büscher, and C. Lange, *Eur. Phys. J. Plus* 131, 19 (2016).
31. Post Irradiation Examination Guide, Idaho National Laboratory report INL/MIS-15-35828 (2015).
32. J.M. Harp, L. Capriotti, and H.J.M. Chichester, *J. Nucl. Mater.* 515, 420 (2019).
33. M. Teague, B. Gorman, J. King, D. Porter, and S. Hayes, *J. Nucl. Mater.* 441, 267 (2013).
34. D.L. Porter and H. Tsai, *J. Nucl. Mater.* 427, 46 (2012).
35. M.K. Meyer, J. Gan, J.F. Jue, D.D. Eeiser, E. Perez, A. Robinson, D.M. Wachs, N. Woolstenhulme, G.L. Hofman, and Y.S. Kim, *Nucl. Eng. Technol.* 46, 169 (2014).
36. D.M. Wachs, A.B. Robinson, F.J. Rice, N.C. Kraft, S.C. Taylor, M. Lillo, N. Woolstenhulme, and G.A. Roth, *J. Nucl. Mater.* 476, 270 (2016).
37. W.J. Williams, A.B. Robinson, and B.H. Rabin, *JOM* 2546 (2017).
38. F. Rice, W. Williams, A. Robinson, J. Harp, M. Meyer, and B. Rabin, Idaho National Laboratory report INL/EXT-14-33066 (2015).
39. A.E. Craft, W.J. Williams, M.I.K. Abir, and D.M. Wachs, Idaho National Laboratory report INL/EXT-13-30741 (2013).
40. A.E. Craft, D.M. Wachs, M.A. Okuniewski, D.L. Chichester, W.J. Williams, G.C. Papaioannou, and A.T. Smolinski, *Phys. Proc.* 69, 483 (2015).
41. A.E. Craft, G.C. Papaioannou, D.L. Chichester, and W.J. Williams, *Phys. Procedia* 88, 81 (2017).
42. A.E. Craft, and B. Schillinger, WCNR-11 in Materials Research Proceedings. Submitted for publication (2019).
43. A.E. Craft, C. Grünzweig, M. Morgano, and E. Lehmann, WCNR-11 in Materials Research Proceedings. Submitted for publication (2019).
44. DOE Standard "Preparation of Nonreactor Nuclear Facility Documented Safety Analysis", DOE-STD-3009-2014, November 2014.
45. Accelerator Facility Safety Implementation Guide for DOE O 420.2C, Safety of Accelerator Facilities, US Department of Energy, Office of Science, DOE G 420.2-1A, August 1, 2014.
46. H.R. Wenk, L. Lutterotti, and S. Vogel, *NIMA* 515, 575 (2003).
47. S.C. Vogel, C. Hartig, L. Lutterotti, R.B. Von Dreele, H.R. Wenk, and D.J. Williams, *Powd. Diffr.* 19, 65 (2004).
48. S. Takajo and S.C. Vogel, *J. Appl. Cryst.* 51, 895 (2018).
49. A.S. Losko, S.C. Vogel, H.M. Reiche, and H. Nakotte, *J. Appl. Cryst.* 47, 2109 (2014).
50. M. Mocko, G. Muhrer, and F. Tovesson, *NIMA* 589, 455 (2008).
51. M. Mocko and G. Muhrer, *NIMA* 704, 27 (2013).
52. A.S. Tremsin, J.B. McPhate, J.V. Vallerger, O.H. Siegmund, W.B. Feller, E. Lehmann, and M. Dawson, *NIMA* 628, 415 (2011).
53. A.S. Tremsin, J.B. McPhate, J.V. Vallerger, O.H. Siegmund, W.B. Feller, E. Lehmann, L.G. Butler, and M. Dawson, *NIMA* 652, 400 (2011).
54. A.S. Tremsin, W. Kockelmann, D.W. Pooley, and W.B. Feller, *NIMA* 803, 15 (2015).
55. N.M. Larson, *Updated Users' Guide for SAMMY Multilevel R-matrix Fits to Neutron Data Using Bayes' Equation* (Oak Ridge: Oak Ridge National Laboratory, 1998).
56. M.C. Moxon, T.C. Ware, and C.J. Dean, REFIT-2009 A Least-Square Fitting Program for Resonance Analysis of Neutron Transmission. Capture, Fission and Scattering Data Users' Guide for REFIT-2009-10 (UKNSFP243, 2010).
57. C. Messaoudil, T. Boudier, C.O. Sorzano, and S. Marco, *BMC Bioinform.* 8, 288 (2007).
58. A.S. Tremsin, A.E. Craft, M.A. Bourke, A.T. Smolinski, G.C. Papaioannou, M.A. Ruddell, J. Littell, and J. Tedesco, *NIMA* 902, 110 (2018).
59. A.S. Tremsin, A.E. Craft, G.C. Papaioannou, A.T. Smolinski, N.M. Boulton, M.A. Ruddell, B.J. Littell, and K.D. Riley, *NIMA* 927, 109 (2019).
60. S.H. Giegel, C.L. Pope, and A.E. Craft, *NIMB* 454, 28 (2019).
61. L. Yin, B.J. Albright, B.M. Hegelich, K.J. Bowers, K.A. Flippo, T.J. Kwan, and J.C. Fernández, *Phys. Plasmas* 14, 056706 (2007).
62. T.P. Wangler, Los Alamos Scientific Laboratory report LA-8388, TRN: 81-001972 (1980).
63. S.C. Vogel, M. Roth, J.C. Fernandez, D.C. Gautier, and K.F. Schoenberg, *Neutron News* 29, 32 (2018).
64. A.S. Tremsin, A.S. Losko, S.C. Vogel, D.D. Byler, K.J. McClellan, M.A. Bourke, and J.V. Vallerger, *AIP Adv.* 7, 015315 (2017).

Publisher's Note Springer Nature remains neutral with regard to jurisdictional claims in published maps and institutional affiliations.